3D Reconstruction of Tubular Structures from Three Orthogonal MRI Projections

Junmo An[1], Mahmut Unan[1], Karen Chin[2], Dipan J. Shah[2], Andrew G. Webb[3], Ioannis Seimenis[4], and Nikolaos V. Tsekos[1]

[1] Medical Robotics Laboratory, University of Houston, Houston, TX, USA
[2] Methodist DeBakey Cardiology Associates, Houston Methodist, Houston, TX, USA
[3] C.J. Gorter Center for High Field MRI, Leiden University Medical Center, Leiden, Netherlands
[4] Laboratory of Medical Physics, Department of Medicine, Democritus University of Thrace, Alexandroupolis, Greece

Abstract— **This study presents a novel method for 3D imaging of tubular structures, such as blood vessels and catheters. With this method, the 3D object is reconstructed from three mutually exclusive orthogonal projections of the same volume. This triplanar projection imaging (TPI) was evaluated on a phantom filled with T1-shortening, Gd-based contrast agent embedded into a matrix. The projected structures were segmented out on each one of the projections and a backprojection algorithm was used to generate a rendering of the tubular structure in 3D. The accuracy of the method was investigated by comparing the centerline of the 3D tubular structure generated from TPI with the centerline extracted from a multislice set of images of the same volume. The two tubular structures were well matched in 3D. With further optimization and reduction of acquisition time, this method can be used for 3D fast imaging of interventional tools or blood vessels with applications in interventional MRI.**

Keywords— **Magnetic resonance imaging, contrast enhanced, 3D reconstruction, volumetric imaging, projection imaging.**

I. INTRODUCTION

Since the superb soft-tissue contrast of the MRI is unparalleled by other imaging modalities, many endeavors have been devoted to the development of MR-guided interventions [1, 2]. The multiplanar capabilities of MRI provide multislice and/or volumetric imaging for excellent visualization of the interventional procedure region of interest.

Although MRI is a very versatile and powerful diagnostic tool modality, it cannot provide, due to its inherent relatively low sensitivity, instantaneous speed and high spatial resolution afforded with x-ray based modalities such as fluoroscopy and angiography. 3D reconstruction from two projections is well studied in biplane fluoroscopy [3, 4]. In fluoroscopic imaging cases where the two projections that are not orthogonal to each other and the centers of the corresponding field of views (FOVs) are not identical, a series of transformations is applied to coregister the two projections to a common coordinate system of reference. With MRI, the multiple projections are already inherently coregistered, and the center and size of the FOVs are identical. The inherent coregistration and coincidence of the FOV of the multiple projections result in a rather simple geometric processing. With 2D multislice MRI, however, the speed of imaging and 3D visualization is rather slow. Multiple projection imaging methods were proposed for 3D visualization of active catheters [5-8]. In this study, in order for planning and guiding interventional devices, we investigate fast volumetric reconstruction of targeted contrast enhanced (CE) tubular structures, such as catheters and blood vessels, with a simultaneously collecting method - triplanar projection imaging (TPI).

II. MATERIALS AND METHODS

A. Triplanar Projection Imaging (TPI)

3D reconstruction of an imaged structure entails two independent but interrelated processes. First, the acquisition of the projections and, second, the reconstruction of the structure in the 3D space. Originating from its inherent 'true-3D' capabilities, MRI provides certain benefits in collecting data and facilitating the 3D reconstruction of the imaged structure from its projections: (a) The inherent coregistration of the spatial encoding on the three projections makes axes assignment and matching straightforward. (b) The orientation of the imaged volume can be set to any arbitrary plane relative to the structure which can be used to better resolve it, thus reducing the number of needed projections and computational resources required from the reconstruction algorithm. (c) The angle between the projection planes can be adjusted to any desired value and is not limited to orthogonal. Figure 1(a) illustrates the operation of the method that collects three projections by setting the thickness of the slice in each acquisition (Fig. 1(b)) equal to the FOV encoded by the phase and readout gradients.

B. TPI Acquisition

Without loss of generality, we hypothesize that the interest is to visualize the tubular structure of choice without any background signal. This can further simplify the segmentation and the 3D reconstruction of the structure. In the experimental part, therefore, we filled the tubular structure with T1-shortening Gd agent and used magnetization preparation to the implemented sequences to achieve long T1 species background suppression.

E. Kyriacou et al. (eds.), *XIV Mediterranean Conference on Medical and Biological Engineering and Computing 2016*,
IFMBE Proceedings 57,
DOI: 10.1007/978-3-319-32703-7_64

The TPI sequence was evaluated on a phantom made of a Gd-filled (3% Gd-doped water) tube (3.0 mm inner diameter and 4.0 mm outer diameter) embedded into a fat matrix of 53% vegetable oil. MR projection images were obtained using a 1.5T whole body MRI scanner (MAGNETOM Avanto, Siemens AG, Medical Solutions, Erlangen, Germany) and the standard built-in body coil was used for transmit/receive. First, a 2D multislice set of 128 coronal slices was collected as a reference with a standard inversion recovery gradient recalled echo (GRE) sequence (TR/TE = 3.8/1.52 ms, flip angle = 40°, bandwidth/pixel = 592 Hz, matrix size = 384X264, FOV = 191X131 mm^2, slice thickness = 1.3 mm). Then three projections (i.e., a TPI set) were collected along the sagittal, transverse and coronal planes with a T1 weighted fast imaging with a steady-state precession (TrueFISP) pulse sequence (TR/TE = 26.07/3.71 ms, flip angle = 75°, bandwidth/pixel = 250 Hz, matrix size = 256X256, FOV = 200X200 mm^2, slice thickness = 200 mm).

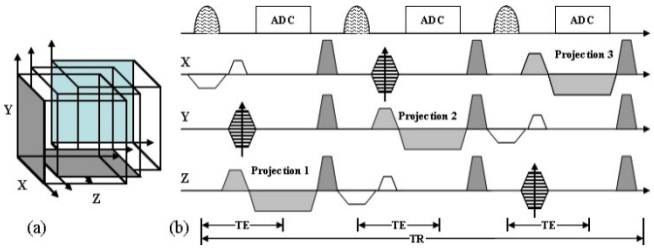

Fig. 1 Acquisition method of three projection images - repetition time (TR) echo time (TE) and analog-to-digital converter (ADC)

C. 3D Reconstruction

Figure 2 is the flowchart of the process followed to generate the 3D reconstruction of the structures from a TPI set: (a) acquisition of the three orthogonal projections, (b) segmentation of the contrast enhanced structure in the three projections, (c) backprojection of segmented objects into the 3D volume, (d) calculation and 3D reconstruction of the intersection volume from the three backprojected objects, and (e) calculation of the centerline curve. This processing was performed offline with code implemented in MATLAB.

The algorithm for the segmentation of the structure in each 2D projection included sharpening, edge detection, and object boundary segmentation. First, to enhance the boundaries of the tubular structure (i.e., versus the background matrix) we applied unsharp masking [9]. Edge detection was then followed that was based on the Sobel operator [10]. Finally, object boundary segmentation was applied, based on the Legendre Level Set algorithm to detect the boundaries of the tubular structure on each projection image [11]. The parameters for each process, such as the region and position of the initialization mask for object boundary segmentation, were manually adjusted on the software GUI.

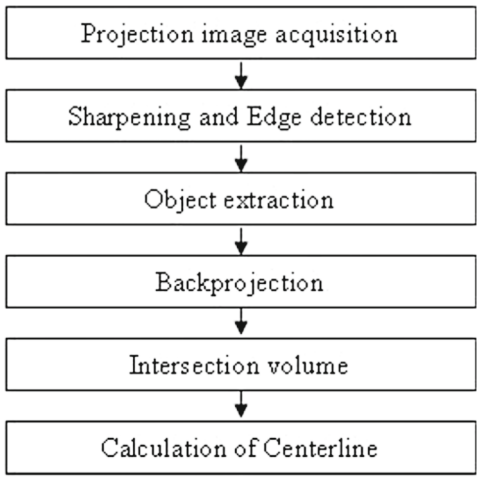

Fig. 2 Flowchart of the 3D reconstruction process

The segmented structures on each one of the three projections were then backprojected along the X axis for the sagittal (Y and Z scanner axes), the Y axis for the coronal (X and Z scanner axes) and the Z axis for the transverse (X and Y scanner axes) projections. The intersection volume of the three backprojections was calculated with Algorithm 1. With this algorithm, intersection points were calculated from point sets (i.e., $\boldsymbol{p_C}$ of coronal, $\boldsymbol{p_S}$ of sagittal, and $\boldsymbol{p_T}$ of transverse) in set $\boldsymbol{B_C}$ of coronal, $\boldsymbol{B_S}$ of sagittal, and $\boldsymbol{B_T}$ of transverse backprojected volumes with a logical AND operator. 3D volume model of a tubular structure was extracted using the marching cube algorithm [12].

Algorithm 1. Match driven backprojections

input: B_C, B_S, B_T
output: M

```
for each point p_T in B_T
    for each point p_S in B_S
        for each point p_C in B_C
            if p_C & p_S & p_T = 1 then
                M ← p_C
            end if
        end for
    end for
end for
```

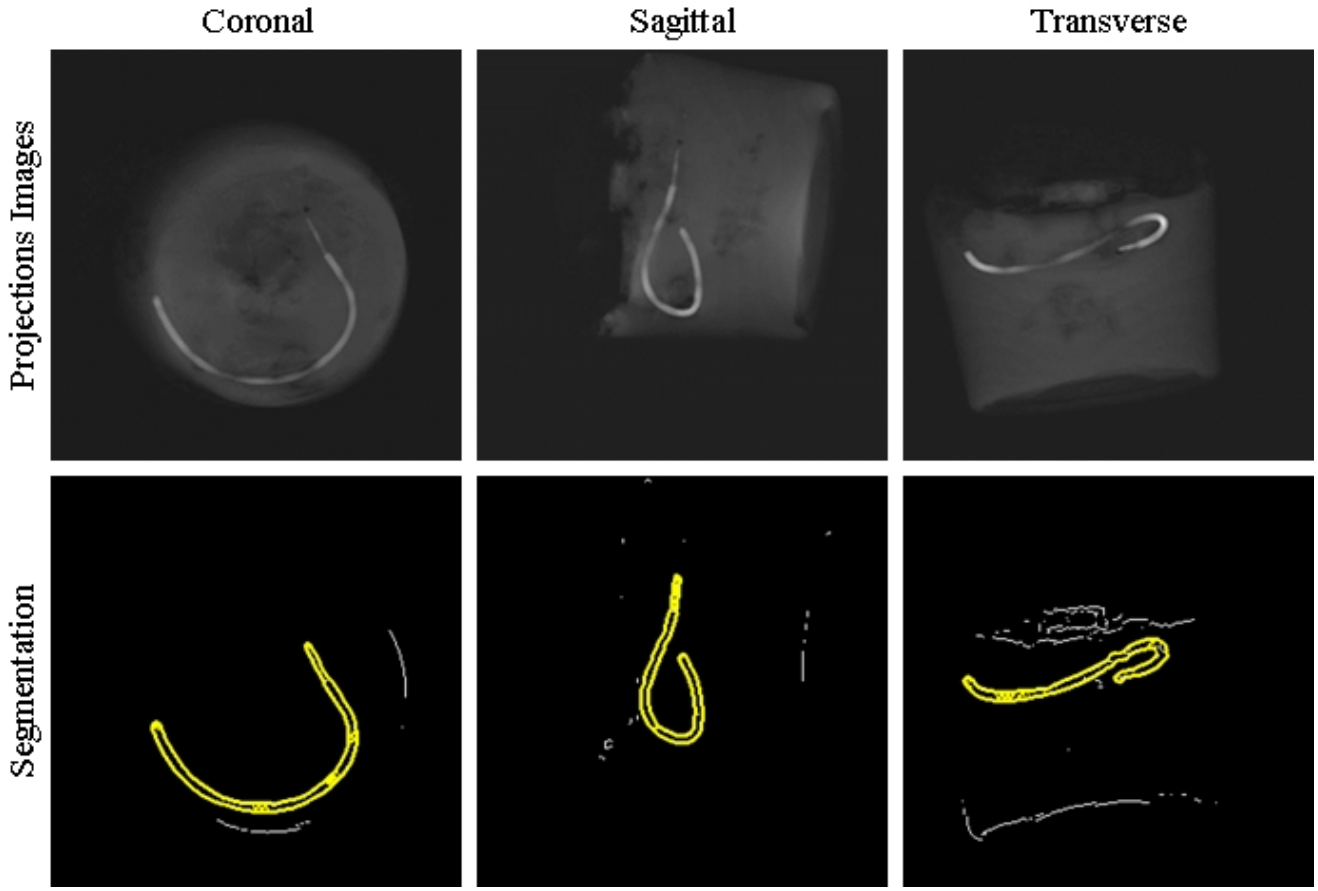

Fig. 3 The three projection images acquired (upper row), and the result after edge detection and segmentation (lower row)

D. Data Processing

The 3D object reconstructed from the TPI data was compared to the object reconstructed from the multislice (128 slices), that was also generated with the exact same segmentation algorithm. The voxel data were stored in 3D array structures to extract the polygonal meshes of the isosurfaces with marching cubes. Skeleton extraction, based on the L1-medial skeleton algorithm [13], was then performed to extract the corresponding centerlines of the two 3D renderings of the tubular structures. The skeleton extraction algorithm also calculates the minimum number of points required to generate the centerline of the structure. In general, this number depends on the 3D shape and size of the structure [13]. For the shapes extracted from the TPI and multislice datasets, the algorithm retuned a minimum of 38 points that was used in all processing. For each point on both skeletons we calculated the coordinates (X_{3d}, Y_{3d}, Z_{3d}) and (X_{msl}, Y_{msl}, Z_{msl}), where '3d' are the coordinates of the points on the centerline generated from the TPI and 'msl' of the corresponding points on the centerline from the multislice set, their differences along the three axes and their Euclidean distance $\text{sqrt}[(X_{3d}-X_{msl})^2 + (Y_{3d}-Y_{msl})^2 + (Z_{3d}-Z_{msl})^2]$. Those values were then reported as averages and standard deviations (for n = 38).

III. Results

Figure 3 displays the original unprocessed 2D projections (upper row) and the corresponding segmentation results (lower row). This processing was based on the assumption that the background signal from the fat matrix was sufficiently saturated; therefore, it is possible to segment out the tubular structure. While those data were successful in the reconstruction of the 3D structures, there are some notable limitations. The background signal was not fully suppressed. The signal intensity (SI) of the contrast enhanced structure was 39.44 ± 11.48 as compared to a matrix SI of 16.06 ± 4.07. Suboptimal suppression of the background matrix SI occurred because of (1) the imperfect inversion of the inversion recovery magnetization preparation module of the pulse sequence used that was employing a non-selective RF pulse, (2) the background signal originates from a total

volume of 200x200x200[3]; therefore, any unsuppressed signal adds to a large value. Also, preparation of the phantom was not ideal since air was trapped giving rise to the signal artifacts that resulted to the isolation of other background structures (especially, seen in the transverse slice) that were manually removed before backprojections.

Figure 4 displays the 3D rendering of the tubular structure reconstructed from the TPI set using Algorithm 1, together with the three acquired projections. The reconstructed structure has the shape of the original object as compared to the arrangement of the tube inside the phantom.

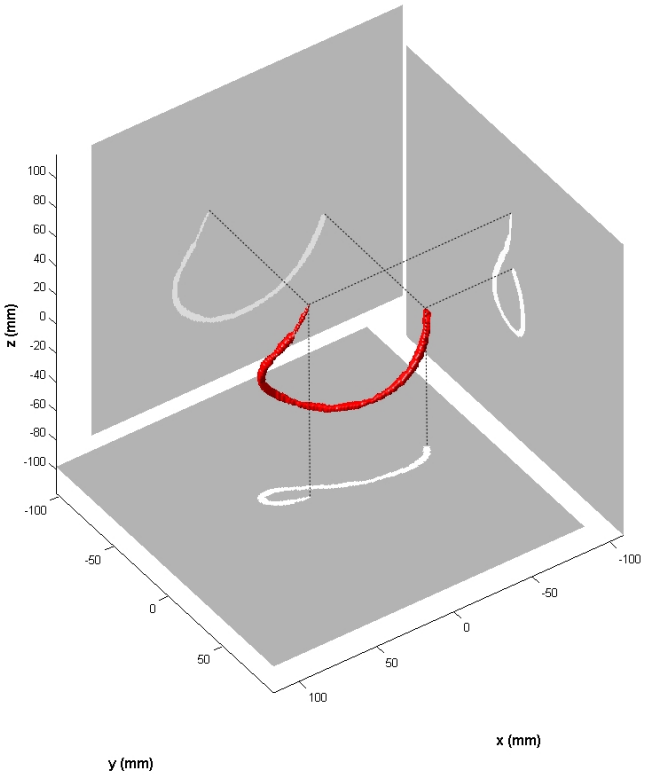

Fig. 4 TPI-based 3D surface rendering of the tubular structure and the corresponding three orthogonal 2D projections

Figures 5 and 6 show and compare superimposed the two 3D centerlines generated by the TPI and the multislice set demonstrating, in qualitative terms, a good matching of the two curves. Although the two data sets were collected with different resolutions (the pixel size for the multislice set is 0.48 mm and for the TPI is 0.78 mm), some quantitative appreciation of their matching can be calculated. Specifically the 3D Euclidean distance between their points was 1.73 ± 0.80 mm. The differences on the corresponding X, Y and Z axis coordinates were 1.21 ± 0.83 mm, 0.56 ± 0.41 mm and 0.84 ± 0.55 mm, respectively. It appears that the largest difference in the matching of the two centerlines originates from the X axes as can also be appreciated in Figs. 5 and 6.

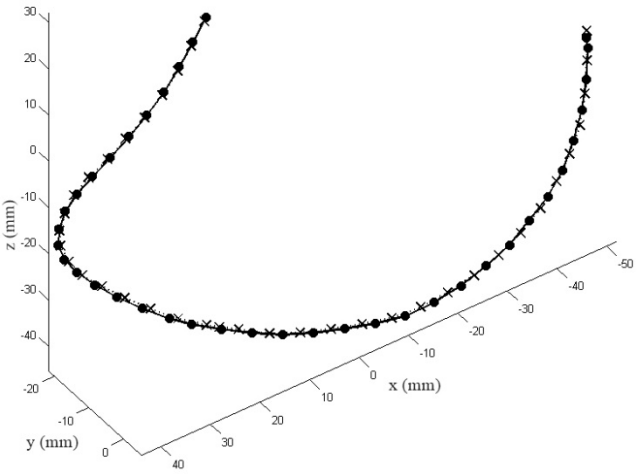

Fig. 5 Comparison of the centerlines of the 3D renderings generated from the three projection images (solid line with circle markers) and from the multislice MR images (dotted line with cross markers)

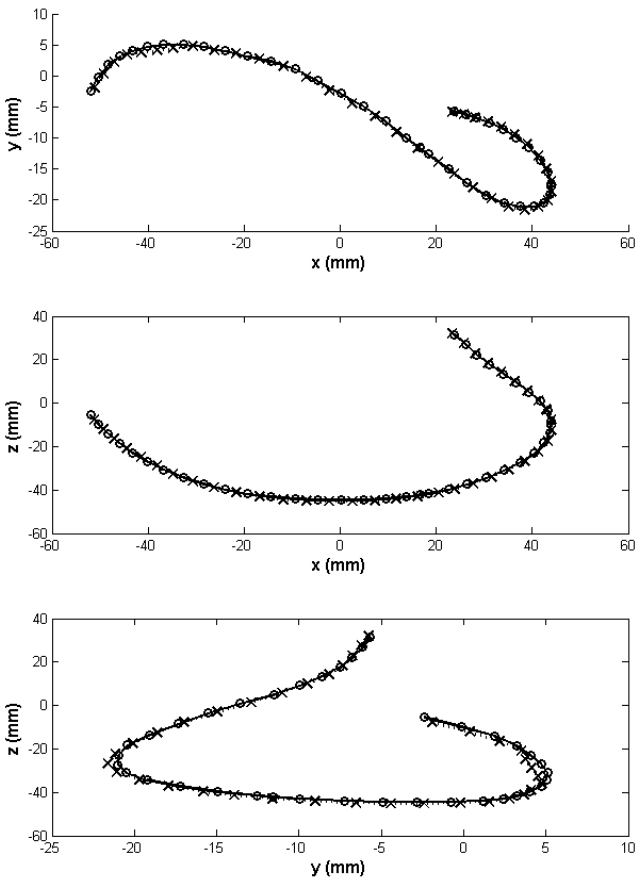

Fig. 6 Comparison of the centerlines as projected onto the three orthogonal planes

IV. Discussion

This work introduces and describes proof-of-concept studies of an MRI method to image tubular structures from a set of three orthogonal 2D projections. The method is similar to biplane x-ray fluoroscopy. However, MRI offers certain benefits originating from the inherent to the modality and direct coregistration of the three projections. This is unlike the x-ray fluoroscopy which requires spatial transformations to correlate the spatial coordinates on the two projections and appropriate adjustment of the size of the structure to account for the different distances of the x-ray sources and detectors.

The feature of MRI for computer controlled selection of oblique volumes can be used to collect the TPI with any desired orientation in space to better resolve complex structures. With the state-of-the-art scanners, dynamic adjustment of the acquisition parameters, including the gradient axis is possible. Thus, the scanner may be dynamically adjusted on-the-fly by the operator or by an automated scheme in between acquisitions each with different orientations of the TPI planes. An example has been shown before when a robot was controlling on-the-fly the MRI imaging plane [14].

The accuracy of 3D reconstruction of the imaged structures from TPI depends on the accurate matching of the three projections. The reconstruction is determined primarily by the performance of the spatially encoding magnetic field gradients. Potential suboptimal gradient performance may result in mismatching of the encoding axis and the reconstructed object may be mismatched and distorted when compared to the actual structure. Shape distortion will also occur if the readout encoding axes are not perfectly prescribed or the gradients do not perform as expected. Of course, those are spatial misregistration problems which can be encountered to any pulse sequence and depend on the performance of the hardware. Another aspect of the reconstruction is the coincidence of the excited volumes. The TPI pulse sequence can be susceptible to mismatch of the excitation volumes. This requires that the excitation frequency and the excitation bandwidths of the pulses be accurately prescribed to avoid excitation intensity gradients secondary to the pulse profiles. It should be mentioned that this problem can be eliminated by using non-slab selective excitation or if the slab selection gradients are along the same axis, e.g., X axis, so the excitation profiles of all pulses are identical.

A central aspect of the implemented TPI sequence is the suppression of the background signal which originates from all structures but the contrast enhanced one. Suppression is used for two interrelated reasons: to improve contrast and simplify the reconstruction. With non-selective or thick-slab excitation, signal is collected from a large volume and if not suppressed it can be substantial relative to the contrast enhanced structure. The importance of efficient background suppression in dynamic magnetic resonance angiography (MRA) for improved vessel-to-tissue contrast-to-noise ratio (CNR) with projection or thick-slab MRA has been demonstrated before [15, 16]. A direct consequence of the reduced contrast can be the virtual masking of the targeted structure precluding or making challenging its segmentation, and therefore reconstruction. In the presented work, we used a short duration magnetization preparation to harvest the highest possible signal from the short T1 species (i.e., the contrast enhanced structure) while saturating the long T1 background.

Example applications of the TPI are the dynamic imaging of contrast enhanced vessels, and passive tracking and imaging of catheters, and other flexible or rigid interventional devices such as endoscopes equipped with contrast agent filled markers. The primary feature of the TPI acquisition is the volumetric imaging of a structure with the concurrent elimination of the background.

V. Conclusions

This work demonstrates the implementation of an acquisition scheme for volumetric imaging of contrast enhanced tubular structures with the simultaneous collection of three orthogonal projections. The tested TPI sequence provided spatial matching of the structure in the three projections, as benchmarked against a conventional multislice technique. A simple algorithm provided accurate 3D reconstruction of the object. Further development and evaluation is underway to implement faster TPI pulse sequences, develop reconstruction code for real-time online reconstruction (in C/C++) and accelerated visualization on a Graphics Processor Unit (GPU) for interactive 3D visualization on-the-fly. In addition, assessment of the method for reconstructing more complex structures followed by in vivo studies are warranted. Among other applications, TPI sequences can be used to visualize contrast enhanced catheters and vessels, as well as tubular MR-visible markers on interventional tools and manipulators.

Acknowledgment

This study is supported by the National Science Foundation award (CNS-0932272).

Conflict of Interest

The authors declare that they have no conflict of interest.

REFERENCES

1. Tsekos NV, Shudy J, Yacoub E et al. (2001) Development of a robotic device for MRI-guided interventions in the breast, Proc. IEEE Int Symp Bioinform Bioeng pp. 201-208
2. Tsekos NV, Ozcan A, Christoforou E. (2005) A prototype manipulator for magnetic resonance-guided interventions inside standard cylindrical magnetic resonance imaging scanners. J Biomech Eng 127 (6):972-80
3. Baert SA, van de Kraats EB, van Walsum T et al. (2003) Three-dimensional guide-wire reconstruction from biplane image sequences for integrated display in 3-D vasculature. IEEE Trans Med Imaging 22 (10):1252-8
4. Bender HJ, Manner R, Poliwoda C et al. (1999) Reconstruction of 3D Catheter Paths from 2D X-ray Projections, Proc. MICCAI vol. 1679, pp. 981-989
5. Solaiyappan M, Lee J, Atalar E. (1999) Depth Reconstruction from Projection Images for 3D Visualization of Intravascular MRI Probes, Proc. ISMRM
6. Sathyanarayana S, Aksit P, Arepally A et al. (2007) Tracking planar orientations of active MRI needles. J Magn Re-son Imaging 26(2):386-391
7. George AK, Derbyshire JA, Saybasili H et al. (2010) Visualization of active devices and automatic slice repositioning ("SnapTo") for MRI-guided interventions. Magn Reson Med 63(4):1070-9
8. Schirra CO, Weiss S, Krueger S et al. (2010) Accelerated 3D catheter visualization from triplanar MR projection images. Magn Reson Med 64(1):167-76
9. Polesel A, Ramponi G, Mathews VJ (2000) Image enhancement via adaptive unsharp masking, IEEE Transactions on Image Processing, vol. 9, pp. 505-510
10. Chaudhuri S, Chatterjee S, Katz N et al. (1989) Detection of blood vessels in retinal images using two-dimensional matched filters, IEEE Transactions on Medical Imaging, vol. 8, pp. 263-269
11. Mukherjee S, Acton S (2015) Region Based Segmentation in Presence of Intensity Inhomogeneity Using Legendre Polynomials, IEEE Signal Processing Letters, vol. 22, is-sue 3, pp. 298-302
12. Lorensen WE, Cline HE (1987) Marching Cubes: A High Resolution 3D Surface Construction Algorithm, Proc. SIGGRAPH vol. 21, pp. 163-169
13. Huang H, Wu S, Cohen-Or D et al. (2013) L1-Medial Skeleton of Point Cloud, Proc. SIGGRAPH vol. 32, pp. 65:1-8
14. Christoforou E, Akbudak E, Ozcan A et al. (2007) Performance of interventions with manipulator-driven real-time MR guidance: implementation and initial in vitro tests. Magn Reson Imaging 25(1):69-77
15. Yamashita Y, Abe Y, Tang Y, Urata J et al. (1997) In vitro and clinical studies of image acquisition in breath-hold MR cholangiopancreatography: single-shot projection technique versus multislice technique. AJR Am J Roentgenol 168(6):1449-54
16. Atalar E, Kraitchman DL, Carkhuff B et al. (1998) Catheter-Tracking FOV MR Fluoroscopy. Magn Reson Med 40(6):865-72

Author:	Nikolaos V. Tsekos
Institute:	Medical Robotics Laboratory, University of Houston
Street:	501 Philip G. Hoffman Hall
City:	Houston, TX
Country:	U.S.A.
Email:	nvtsekos@central.uh.edu